

**Deliverable #6 - RFQ 04-01 C07**  
**“Safety Assessment of Steel Bridges**  
**Damaged by Truck Strikes”**

**Task F - Final Report**

C. J. Earls\*      C. J. Stull†

February 22, 2007

---

\*Associate Professor, School of Civil and Environmental Engineering, 220 Hollister Hall,  
Ithaca, NY 14853

†Doctoral Student, School of Civil and Environmental Engineering, 220 Hollister Hall,  
Ithaca, NY 14853

## 1 Executive Summary

Slab-on-steel stringer bridge systems are a staple in our Nations surface transportation system. Unfortunately, it is somewhat common to have a scenario wherein an over-height truck encounters a particularly low bridge; subsequently leading to a truck strike to the overhead steel superstructure.

Given the mass of typical trucks, coupled with the high velocity associated with interstate travel, relatively large amounts of kinetic energy can be transmitted to the overhead bridge during such a truck strike event. Typically, the slab-on-steel stringer bridge will dissipate this energy through the development of plastic deformations in the steel stringers (leading to twisted and / or dented flanges as well as out-of plumb girder webs); plastic buckling of cross-frame and diaphragm members; unwanted relative motions at the bearings leading to mis-alignments between the superstructure and the underlying substructure; and in the case of composite slab to steel stringer systems, damage to the composite action occurring at the steel-to-concrete interface. Correctly assessing this damage and arriving at a rational means for determining reserve capacity in the damaged system presents a formidable challenge to the bridge engineer. Stability is a very important theme within the context of strength evaluation due to the fact that large initial imperfections may now be present throughout the damaged bridge system, and also since previously effective bracing members, may now be compromised as a direct result of the damage that they sustained during the event.

The following describes, and reports on, results from a research program involving multiple laser scanning technologies that are coupled with the latest image processing techniques to provide reliable, high resolution point cloud data sets suitable for constructing detailed solid models of the structural system. The solid models are themselves suitable for meshing and analysis with state-of-the-art commercial multi-purpose nonlinear finite element software systems such as ADINA.

## 2 Introduction

The problem of assessing steel I-girder bridge systems damaged by catastrophic events (e.g. over-height truck strikes) is one for which conventional analysis approaches do not readily present a practical and efficient solution. While it is that the behavior of an undamaged structure is readily obtainable through analytical models that consider as-built drawings, inspection reports, etc., post-event structures possess geometric and / or mechanical anomalies (e.g. out-of-plane deformations, residual stresses, etc.) which can rarely be accounted for given the assumptions employed in typical design office analysis procedures. Furthermore, characteristic differences between structures, as well as damage configurations, make the standardization of such an analysis procedure nearly impossible. As a result, the current solution to this problem relies on “engineering judgement,” which, in its purest form, is simply an opinion. The aim of the research program reported upon herein is to explore the applicability of a proposed technique to rapidly *and* accurately assess bridges damaged by over-height truck strikes.

This proposed technique adopts an approach to the problem wherein three technologies are merged as follows (Figure 1):

1. terrestrial laser scanning (TLS): obtain a point cloud data set of the structure in its damaged configuration;
2. image processing: derive a parasolid model from this point cloud data set;
3. computational mechanics: determine behavioral characteristics of the damaged structure by integrating this parasolid model into a nonlinear finite element model.

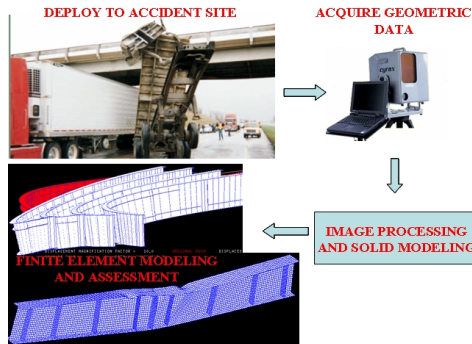


Figure 1: Schematic representation of proposed assessment technique.

An outline of these technologies is provided in the proceeding sections with respect to the subject structure chosen at the onset of this research program: BMS ID No. 62 0070 0244 0624 over SR 0519 in Washington County. For further

information with regard to the selection of this particular structure, Deliverable #1 (Task A - Interim report on selection of a suitable subject structure) is provided in Appendix A of this report.

### 3 Terrestrial Laser Scanning

A thorough discussion of the TLS technologies employed throughout this research program has been submitted to the Commonwealth in the form of Deliverable #2 (Task B - Interim report on validation of data collection and analysis techniques); this deliverable is provided in Appendix B of this report. It is therefore sufficient to provide a general overview of these technologies followed by a thorough discussion of the intrinsic errors associated with TLS technology; the latter of which was not discussed in Deliverable #2.

#### 3.1 TLS System Technologies

The types of TLS systems employed during this research program are: time-of-flight; and continuous wave, or phase-based, systems. The two primary differences between these TLS systems lies in how the beam is emitted from the laser diode and the method of treating the returned signals. In a time-of-flight system, the diode emits a pulsed beam which is reflected off of the target surface back to the system. The difference in *time* between emission and reception of this pulse is then recorded; which is used to compute the stand-off distance between the set-up location and the target surface (Figure 2).

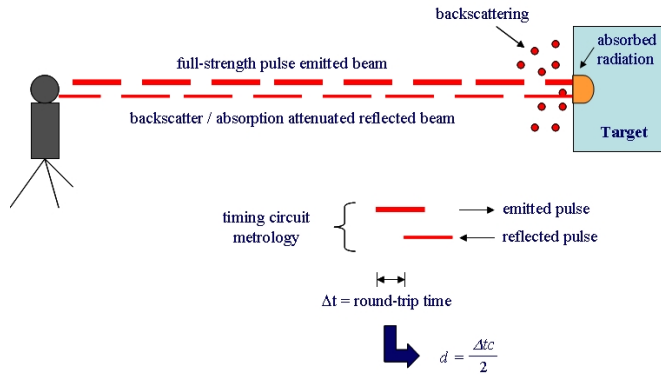


Figure 2: Time-of-flight TLS system.

The continuous wave system, as the name implies, operates with a continuously emitted beam. Determination of the stand-off distance is then based upon the measured *phase-shift* between the emitted and received waves (Figure 3).

With regard to a comparison between these two TLS systems, it has been

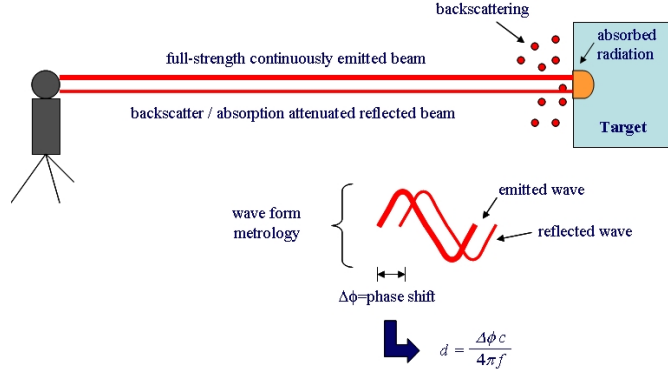


Figure 3: Continuous wave TLS system.

demonstrated that the Zoller + Frohlich (Z+F) Imager 5003 continuous wave system requires approximately one-half of the time, as compared to the CYRAX 2500 time-of-flight system, to acquire raw point cloud data of an entire bridge (the approximate time required by the latter is between 8 and 12 hours). However, it is found in the data analysis portion of this research program that, despite the time savings, the accuracy of point cloud data obtained via the Z+F system is insufficient to develop the previously mentioned parasolid models. Considering that the need for scanning accuracy is vital to this work, only the CYRAX scanner data sets are discussed in this report.

### 3.2 Intrinsic Error

In beginning the discussion of the intrinsic error associated with TLS technology, it is important to first introduce a property of laser radiation known as laser beam dispersion. Laser beam dispersion is a phenomenon wherein the diameter of a laser beam emitted *in air* widens as the distance between the TLS system and the object of interest (e.g. a bridge girder) increases (Figure 4).

It is important to note that this phenomenon is limited to situations in which the laser is emitted in air (i.e. laser beam dispersion will not occur within a vacuum) and varies as a result of temperature, humidity, etc. Clearly, such an effect can have a significant, if somewhat *variable* impact, on the accuracy and resolution of points within a given point cloud data set; depending upon the associated setup location, air quality, etc. Insight into this dispersive effect allows for the proper identification and treatment of erroneous data within individual point cloud data sets; which, in turn, provides an optimal situation for the construction of a parasolid model.

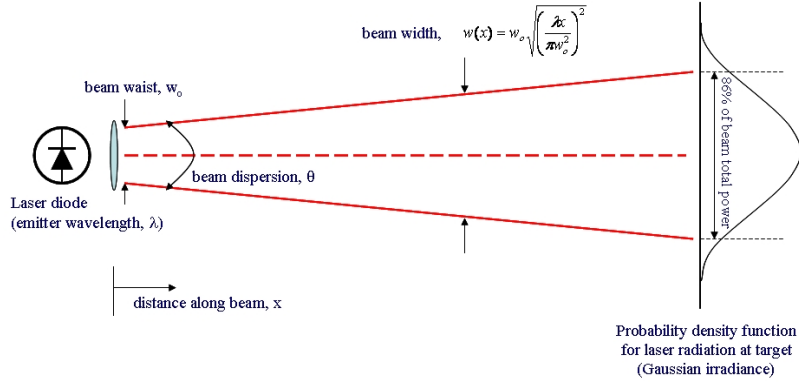


Figure 4: Laser beam dispersion; equation courtesy of [Lichti, et al, 2005]

Within the context of the current research program, there are three sources of error which are of greatest concern: the presence of mixed pixels, multipath error, and error associated with incidence angle. Mixed pixels arise when a single emitted beam is reflected back to the TLS system by two surfaces. Due to the inability of the TLS system to distinguish between these two return signals, an imaginary point, oftentimes referred to as a “phantom point,” is created and stored at a location between these two surfaces, along the beam line-of-sight. Two examples of point clouds with mixed pixels are given in Figure 5; with the latter obtained through work done through this research program.

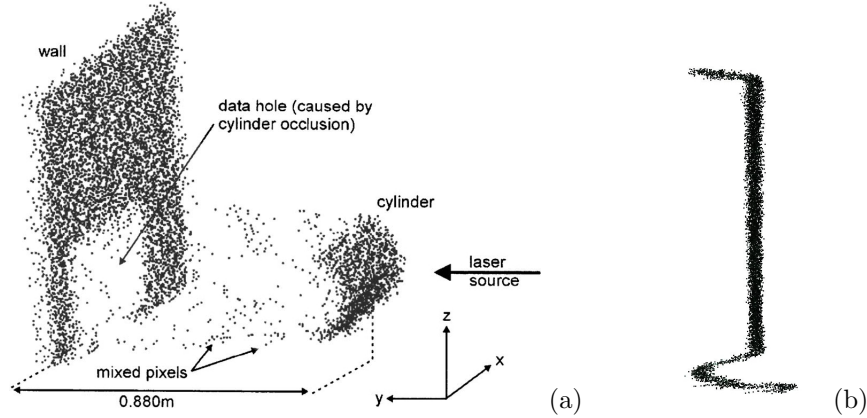


Figure 5: Example point clouds with mixed pixels; (a) cylinder against a wall [Lichti, et al, 2005] (b) cross-section of bridge girder (obtained from Z+F Imager 5003 for this research program).

Multipath error, while more prevalent when scanning highly reflective surfaces, should also be taken into account when considering objects with corners (e.g. flange-web junctions). This type of error is manifested by the backscattering of laser radiation; which in turn produces secondary signals. Such signals are then interpreted by the laser scanning system in a way that causes erroneous data (as illustrated in Figure 6).

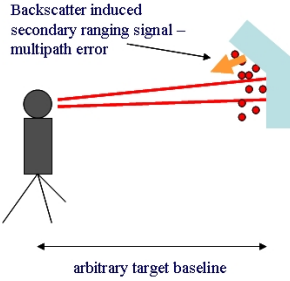


Figure 6: Multipath error.

The final error of interest is that associated with the incidence angle. This angle is a measurement related to the angle formed between the emitted laser beam and the surface normal of the target surface (Figure 7a). Similar in nature to mixed pixels, errors arising from large incidence angles are directly attributed to multiple return signals; the difference lies in that the emitted laser beam strikes *one* surface. However, due to laser beam dispersion, multiple signals (each representing an individual distance) are returned to the TLS system as opposed to a single return signal, as would be the case with a normal surface (Figure 7b).

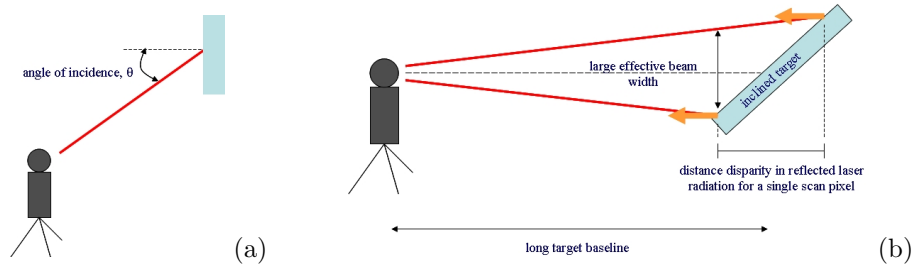


Figure 7: Incidence angle.

It may therefore be deduced that, due to this class of errors, the accuracy of various sub-sets of points within an individual point cloud can vary due to the variation of surface normals and stand-off distances with respect to the scanner set-up locations; this has a significant impact on the automation of the proposed assessment technique. Essentially, a situation arises wherein “accurate”

data must be **manually** parsed from individual point cloud data sets. This, of course, reduces the effectiveness of so-called “all-encompassing” scanner set-up locations in which a large number of structural features are captured in a single point cloud data set (i.e. a small number of all-encompassing scans will typically result in large portions of data being discarded). This condition leads to the conclusion that additional set-up locations are required to map the entire bridge accurately. However, it is pointed out that even with these additional scans, each of the associated point cloud data sets will require parsing so as to arrive at the “cleanest” possible template for parasolid model construction.

## 4 Image Processing

Image processing, in the context of this research program, refers to any operation required to construct a parasolid model, portable to the commercially available finite element software system, ADINA, from a point cloud data set. The individual processes may be summarized as follows:

1. registration of the point cloud data sets with Leica Geosystems HDS Cyclone (the proprietary point cloud data processing software suite associated with the CYRAX scanner);
2. approximation of the damaged region through a partial parasolid model, based upon a point cloud “template”; the commercially available software packages, Geomagic Studio and SolidWorks were employed in this step;
3. construction of the complete parasolid model of the bridge around the parasolid model of the damaged region mentioned previously.

### 4.1 Point Cloud Registration

Registration of the point cloud data provides the primary source of difficulty in this research program. Point cloud data registration is a process in which point clouds which represent multiple regions of a single object (e.g. a bridge) are merged together resulting in a single point cloud of the entire bridge; this step is further complicated by the fact that each scanner set-up location inherits its own local coordinate system.

While it is that the difficulty associated with this step stems primarily from the intrinsic errors discussed in the previous section, a second issue involves the line-of-sight of the TLS system. This is more readily explained through Figure 8 where it may be seen that a set-up at Instrument Position #1 will only capture data from the left side of the left-most girder, and only the bottom portion of the the left side of the right-most girder; the opposite is true for Instrument Position #2.

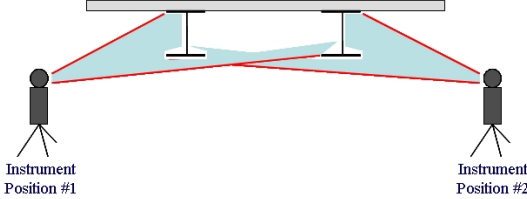


Figure 8: TLS system line-of-sight.

This notion may be applied to an array of bridge girders; thus resulting in the exterior faces of the exterior girders being captured with relative accuracy, while interior girder's point cloud data is sparse, at best. While data from the exterior girders is a primary focus of this work (i.e. most damage from over-height truck strikes occurs to the exterior girders), it was also a goal of this research program to apply this assessment technique to the entire bridge, such that global mis-alignments and modifications from the as-built configuration could be studied as well. Lacking robust point cloud data from the interior portion of the bridge, a global model is not possible unless significantly more time is spent obtaining and registering point cloud data; this violates the research imperative of proposing a rapid assessment technique.

A further issue which stems from the above discussion, is that the point cloud data obtained through the various scanner set-up locations represents *surfaces* which comprise a geometric *volume*. It has already been discussed that, due to the line-of-sight of the TLS system being obstructed by interior girders, obtaining complete data from opposing sides of a girder is nearly impossible. This, of course, further complicates the parasolid modeling process as surfaces must be offset in order to arrive at mid-plane; a non-trivial step when dealing with surfaces derived from point cloud data (Figure 9).

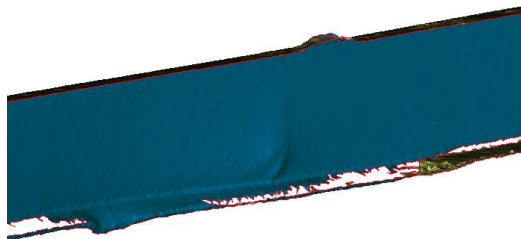


Figure 9: Exterior surface of exterior girder derived from a representative scan; significant and frequent gaps in data occur.

## 4.2 Damage Approximation

Realizing that a global registration of the point cloud data sets obtained for the subject bridge is not practical in most cases, the focus of the research is shifted to utilizing the existing TLS data in a more localized fashion (i.e. supplementing data from bridge plans and as-builts as a mean to treat localized geometric anomalies accompanying damage). This new approach allows for the primary goals of this research program to be realized without requiring numerous scanner set-up locations. In addition, the new approach employs the localized TLS scan data as a sort of template upon which to re-construct the damaged geometry; a sort of reverse engineering of a surface from the point cloud data of the entire bridge using Geomagic Studio. By operating on a more localized scale, not only is computational demand dramatically reduced, but details of the damaged region are more easily accounted for.

## 4.3 Parasolid Model Development

As it is that the ADINA software system is equipped with a complete parasolid kernel, SolidWorks is used to create a solid model of the bridge in parasolid format. Specifically, bridge plans, as-builts, and inspection reports are used to generate the undamaged superstructure components of the subject bridge. Subsequently, the TLS scanner-derived damaged sections created with Geomagic are then inserted into this model in order to complete the formal definition of the overall damaged bridge geometry as a prelude to auto-meshing (described subsequently in Section 5).

# 5 Finite Element Model

The current discussion describing assessment methodology employed in this research project concludes with the development of an analytical model of the bridge in its damaged configuration. The first step in the finite element modeling process involves the geometrical definition of the longitudinal steel girders; by importing the previously discussed solid model into the ADINA User Interface (AUI). In order to expedite the development of the analytical model for this research program, a constant cross-sectional geometry is employed for all girders; the dimensions of this cross-section are obtained through a weighted average of the various as-built cross-sections.

The addition of the concrete deck and transverse steel diaphragms to the analytical model may be achieved through the AUI. The present discussion considers only one of these; others are possible. What is common to all of these approaches for combining finite element idealizations with actual laser scanner - derived topology, is a concern for the *details*. Peculiarities that arise in each of the various steps in the software chain are of enormous importance to a successful modeling effort in the spirit of what is described herein. The subsequent

discussion keeps this perspective in mind as the description of the finite element model construction is given.

### 5.1 Longitudinal Steel Girders

The longitudinal steel girder meshes are composed of shell finite elements defined along the mid-plane of each of the constituent cross-sectional plate components. By applying a finite element mesh consisting of these elements to the solid model, however, a problem is encountered in the flange-web junction at and near the damaged region. Solidworks does not currently have the capability to bind the edge of one surface to the middle of another surface (which results in two disconnected surfaces wherever a flange-web junction occurs). This issue is further complicated in and around the damaged region of the girder due to difficulties in matching the large irregularities presented by the edge and surface (i.e. the bottom edge of the web and the bottom flange).

In the undamaged regions, ADINA's auto-mesher is capable of "tying up" the flange-web junctions through the recognition of coincident nodes. However, within the damaged region, there is a separation between the bottom edge of the web and the center of the bottom flange; such that the auto-mesher cannot reckon a connection. It is therefore necessary to tie these disconnected entities together by way of constraint equations (i.e. enforcing that the two corresponding nodes act as one) defined along the line of elements (Figure 10). An approach such as this ensures mesh compatibility across the elements present at the flange-web junction throughout the damaged region.

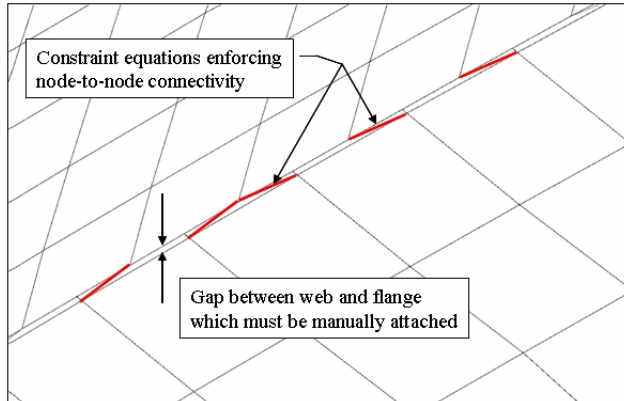


Figure 10: Constraints imposed to insure continuous flange-web junction through damaged region.

## 5.2 Concrete Deck

The marriage of the concrete deck (also composed of shell finite elements) to the top flange of the longitudinal steel girders is achieved by way of node-to-node rigid links; the assignment of a rigid link between two nodes imposes a constraint on the applicable degrees of freedom of the “slave” node such that this node behaves in a kinematically appropriate manner in relation to the displacements of the “master” node. Figure 11 illustrates a representative cross-section of this finite element configuration.

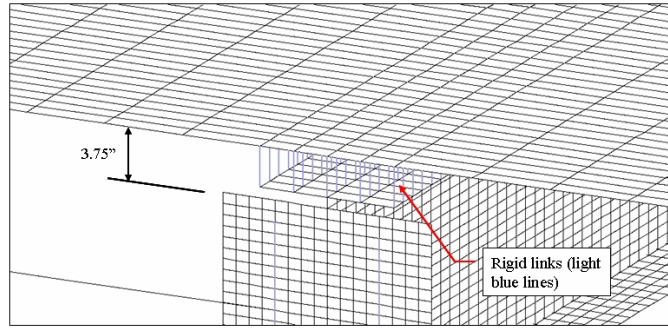


Figure 11: Representative cross-section of the connection between the top flange of the longitudinal steel girders and the concrete deck.

As illustrated in the figure, the shell finite elements which represent the concrete deck are offset from the top flange of the longitudinal steel girders by a distance equal to that of half the depth of the concrete deck (in the present case, 3.75"). This offset, acting in congress with the imposed rigid links, sets these elements in the correct vertical position (i.e. section properties of the composite section are preserved). The thicknesses assigned to these elements are subsequently made to be equal to the actual depth of the concrete deck.

## 5.3 Transverse Steel Diaphragms

To facilitate the development of the finite model, a modeling assumption is implemented with regard to the transverse steel diaphragms. This entails an omission of the steel connector plates specified in the design drawings as a means to connect the transverse steel diaphragms to the longitudinal girder webs; and the insertion of a rigid link configuration as per Figure 12. Such a configuration allowed for the specification of only three girder nodes per diaphragm connection whereas the inclusion of the steel connector plates would likely have entailed hundreds more; thus resulting in a significant time savings. It is further noted that by tying the diaphragm to the top and bottom flange-web junctions, the moment transfer capabilities afforded by the steel connector plates are preserved.

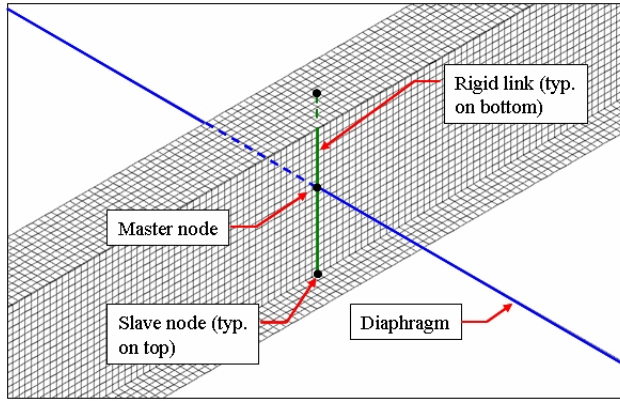


Figure 12: Diaphragm-to-girder connection.

#### 5.4 Material Models

Three material models are employed in the analytical model:

1. a multi-linear inelastic model representing the characteristics of ASTM A7 steel in uniaxial tension and compression;
2. a linear-elastic steel model;
3. a linear-elastic concrete model.

The multi-linear inelastic material model is applied to all shell finite elements which represent steel cross-sections (longitudinal steel girders and stiffener plates). Figure 13 illustrates the stress-strain curve of this material model; additionally, the typical material properties of steel also apply ( $E = 29,500$  ksi,  $\nu = 0.30$ ).

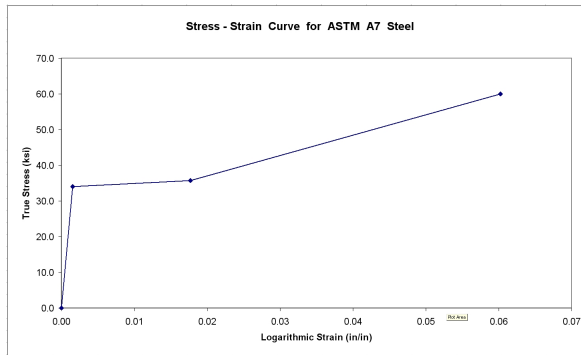


Figure 13: Multi-linear inelastic stress-strain curve for ASTM A7 steel.

All transverse steel diaphragms employ the linear-elastic steel material model. Finally, the material model chosen for the concrete deck is a linear-elastic concrete model with ( $E = 3,122$  ksi,  $\nu = 0.17$ ) which coincides with the minimum specified compressive strength of  $f'_c = 3,000$  psi; design drawings of the subject bridge specified “PennDOT Class A” for the deck concrete. A material model which considers the actual behavioral characteristics of concrete (e.g. high compressive capacity with little to no tensile capacity) is more realistic; however, the authors’ experience in modeling the Lake View Drive bridge failure lead to the decision that such a sophisticated concrete model was not warranted in the present application.

## 5.5 Boundary Conditions

A typical pin-roller boundary condition arrangement is present in the subject bridge. In dealing with longitudinally skewed bridge models, it is expedient to ensure that the local and global coordinate systems coincide: this precludes the need for a separate definition of a local coordinate system at each boundary condition location. It is therefore pointed out that the boundary conditions imposed in this model are as indicated in Table 1 (“x” indicates fixity of the respective degree of freedom).

Location	Degrees of Freedom					
	$u_x$	$u_y$	$u_z$	$\theta_x$	$\theta_y$	$\theta_z$
West Abutment	x	x	x			
Pier 1		x	x			
Pier 1		x	x			
East Abutment	x	x				

Table 1: Fixity of degrees of freedom at support locations.

## 6 Damaged vs. Undamaged Model Comparison

Various analyses of the finite element model discussed in the previous section (i.e. the model of the bridge in its damaged configuration) are conducted to verify the modeling assumptions employed; this process is iterative in nature with the product of these iterations given in the previous section. While a thorough discussion of each step taken during this process need not be included, a secondary benefit of this exercise comes from the comparison against a previously constructed finite element model of the bridge in its as-built configuration. A thorough description of the as-built model may be found in the references [Stull, 2006]. This, of course, provides a means to qualify the reduction in capacity associated with the damaged state, as it compares to the bridge in its undamaged state. It should be noted that the superstructure and substructure of the

subject bridge considered in this research program have previously been rated as “fair” and “satisfactory” [Rhea, 2005]; only the damage due to the multiple truck strikes is considered in the model discussed previously.

The load configuration considered consists of a uniform pressure load applied to the westernmost end span (Figure 14).

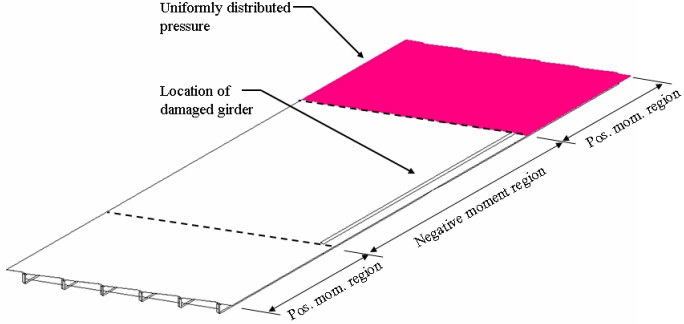


Figure 14: Schematic of load configuration studied.

The motivation behind this load configuration comes from the need to induce a negative moment within the damaged region of the bridge; inducing a positive moment would essentially straighten out the damage at high load levels, resulting in similar ultimate load carrying capacities for the damaged and undamaged models. The state of compression in the bottom flange resulting from the end-span loading, together with the nature of the damage (i.e. significant damage in the out-of-plane direction), presents a condition which is highly unstable when considering lateral buckling.

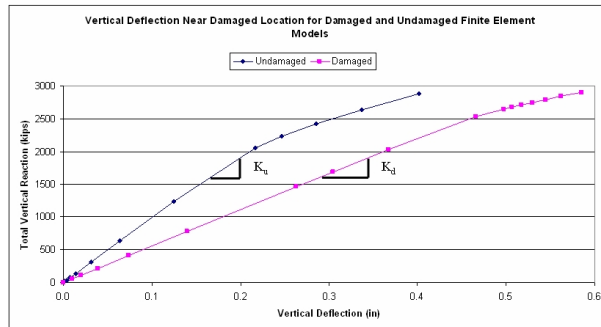


Figure 15: Quantitative comparison of vertical deformation near the damaged region.

Figure 15 is a plot of the upward deflection of a node near the damaged region (an analogous location is chosen for the undamaged model); the y-axis results from the applied pressure multiplied by the area over which it is applied (approximately 1000 square feet in the case of the westernmost end-span), giving the total vertical reaction. As illustrated in this figure, the governing difference between the damaged and undamaged finite element models is that the response of the damaged model is softer in nature than that of the undamaged model. A primary cause for this softened response is illustrated in Figure 16, where the damaged model shows an increased level of lateral deformation than that of the undamaged model.

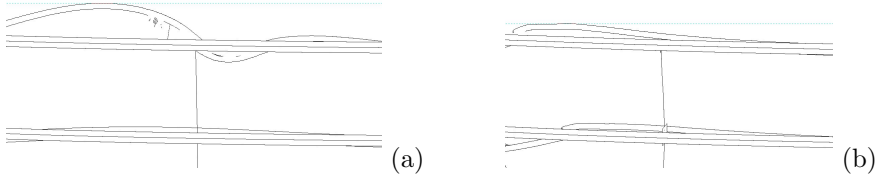


Figure 16: Qualitative comparison of lateral deflection near the damaged region (deformations 100X magnified); (a) damaged bridge model (b) undamaged bridge model.

Further examination of Figure 16 reveals the significant impact of the location of transverse members as they relate to the damaged region; barring the presence of the transverse steel diaphragm within the damaged region, lateral deformations would increase dramatically.

Quantifying the softening response results in an approximately 40 percent relative difference in “stiffness” between the damaged and undamaged models. Calculation of this comparison parameter,  $\epsilon_s$  is achieved through the following equation:  $\epsilon_s = \frac{K_u - K_d}{K_u}$ , where  $K_u$  and  $K_d$  are the slopes of the load-deflection plot for the undamaged and damaged models given in Figure 15, respectively. Considering the level of damage present in the subject structure as well as the modeling assumptions discussed in Section 5, it is recognized that this is likely to be an overestimation of the actual percentage lost. It is again noted that this particular load configuration is chosen to accentuate the instability caused by the damage, thereby resulting in the most extreme reduction in capacity.

As it is that insight into the behavior of the damaged model is of interest, in addition to lateral deformation, it is worthwhile to consider the stress field near the damaged region as well. Figure 17 is provided as means to compare the stress distributions within the model. It can be seen in Figure 17a that the stress distributions for the five southernmost girders are very similar in nature, regardless of the positioning of the transverse steel diaphragm, whereas there is a large rise in stress in the northernmost girder, at the damaged region. This

region of increased stress is on the order of twice that of the other girders, with the extreme stresses equal to or greater than the yield stress of the material (Figure 17b).

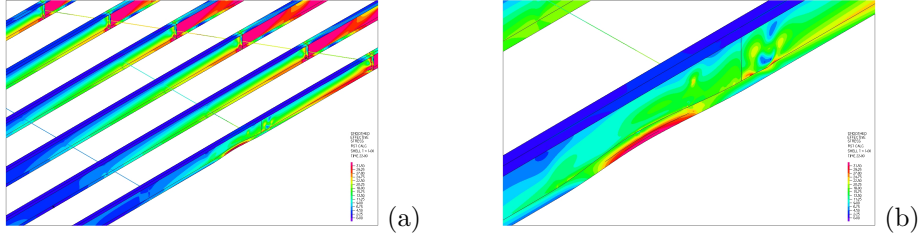


Figure 17: Longitudinal bending stress distributions for damaged model; (a) overall (b) magnification of damaged region.

## 7 Conclusions

The results from a comprehensive research program aimed at the development of a rapid assessment technique for bridge structures damaged by truck strikes has been presented. Such a research program is motivated by the fact that the analysis procedures currently practiced in industry provide results which are approximate at best. Furthermore, it should be noted that these procedures are not standardized, which could result in a situation in which analysis results can vary significantly between engineering offices.

The approach discussed herein provides a robust and useful technique for assessing both the response characteristics of a damaged structure as well as its associated reserve capacity. It is noted that the model discussed in Section 5 also provides significant long-term benefits in that it may be analyzed for load configurations which presents themselves in the future.

This technique, however, is not able to be implemented in an automatic nature. While the challenges imposed by the issues discussed in Sections 3 through 5 are significantly lessened by parsing out the damaged region of the bridge, many of these challenges will still present themselves for application.

Clearly, this research program shows great promise in the way of rapidly assessing damaged bridge structures. However, it has been shown that a considerable effort on the part of knowledgeable engineers possessing background in surveying, laser scanning, image processing, and computational mechanics is required.

## 8 References

1. Lichti, D. D., S. J. Gordon, and T. Tipdecho. "Error Models and Propagation in Directly Georeferenced Terrestrial Laser Scanner Networks." *Journal of Surveying Engineering* 131(2005): 135-42.
2. Rhea Engineers and Consultants, Inc. "SAFETY ASSESSMENT FOR STEEL BRIDGES DAMAGED BY TRUCK STRIKES, BRIDGE INSPECTION REPORT, BMS ID No. 62 0070 0244 0624. 2005.
3. Stull, C.J. "ON THE COMPARISON OF COMPUTATIONAL METHODS FOR ANALYZING LONGITUDINALLY SKEWED STEEL I-GIRDER BRIDGES. MA thesis, University of Pittsburgh, Pittsburgh, Pennsylvania, United States, 2006.

## **9 Appendix A**

### **Deliverable #1 - RFQ 04-01 C07 “Safety Assessment of Steel Bridges Damaged by Truck Strikes”**

#### **Task A - Interim report on selection of a suitable subject structure**

PI Earls from the project team engaged in multiple discussions with District 12-0 personnel regarding possibilities related to a suitable subject steel girder bridge structure that could serve as a focus for the present study. Criteria for selection were related to the following (ranked by importance):

1. The bridge superstructure must be steel.
2. The steel superstructure must be damaged by a truck impact.
3. Access to the underside of the superstructure must be available.
4. Adjacent topography should be such that multiple scans can be made and registered so as to compensate as much as practicable for occluded regions in the superstructure during single scans.
5. Access to a reasonably complete set of bridge plans would be welcomed.
6. Inspection data taken at various times throughout the subject structures service life would be helpful in understanding the evolution of damage within the superstructure.
7. It would be nice if the bridge type, and the damage accumulated, were such that they were too complex for easy assessment by traditional inspection and analysis methodologies.

After discussion with District personnel, the most promising subject bridge was identified as BMS ID No. 62 0070 0244 0624 over SR 0519 in Washington Co (referred to in the remainder as “the Washington County Bridge” or simply as the “subject bridge”). The consideration of each of the seven foregoing criteria is treated within the context of supporting the selection of Washington County Bridge in what follows:

1. The subject bridge is composed of hot-rolled steel sections made from A7 steel. Thus the criterion of a steel superstructure is satisfied.
2. Inspection reports dated 12/7/1995 that were furnished by the District clearly demonstrate a significant amount of damage to the bridge superstructure as a result of truck impacts. Indeed, the inspection report indicates that in the case of the fascia girder opposing southbound traffic on

Route 519, the bottom flange out-of-plane deflections are approximately 7" (this deformation is of the same magnitude as the overall bottom flange width of the W24X76 stringers!) Other data from the inspection report show very significant damage also exists on the fascia girder opposing the northbound traffic on Route 519 as well.

3. Photographs from the site, as well as topological data from the plan set, indicate that the greatest distance from top of grade to the bottom of steel is approximately 15'. This places the steel superstructure at an ideal elevation for the scanning that is to be undertaken as part of this work. Beyond this, the presence of adequate shoulders and adjacent green space prove for safe staging and data collection zones needed to support this work.
4. Please see bullet 3) above for supporting information.
5. The research team was fortunate in that the District was able to furnish the team with a complete set of bridge plans as well as the re-decking plans for the subject bridge.
6. The district has already furnished the research team with an inspection report dated 12/7/1995. It is the research team's understanding that other reports are available, but this is not crucial to the success of the project.
7. The subject bridge is severely damaged and thus offers a significant challenge in properly capturing the salient features of the existing damage for use with the current widely used assessment methods in the engineering office.

However, it will be shown in the present work that these existing tools (i.e. grillage analysis with reduced section, etc.) may prove unsuitable for problems involving damage of this complexity. Beyond this, the subject bridge has a significant skew, and thus, interesting torsional response features will almost certainly evolve and present themselves as a recurring theme as the residual strength within the damaged bridge system is ascertained.

In conclusion, the subject bridge for the present study has now officially been set as BMS ID No. 62 0070 0244 0624 over SR 0519 in Washington Co., PA.

## **10 Appendix B**

### **Deliverable #2 - RFQ 04-01 C07 “Safety Assessment of Steel Bridges Damaged by Truck Strikes”**

#### **Task B - Interim report on validation of data collection and analysis techniques**

Two types of laser scanning technologies are utilized throughout this research program; each based on a slightly different principal of operation: time-of-flight and phase-based systems. The CYRAX time-of-flight ranging system, manufactured by Leica Geosystems HDS LLC, was already owned and operated by the PennDOT District 12-0 Survey Team, thereby presenting a convenient solution to examine the capabilities of this type of non-contact digitizer. In the case of the phase-based ranging system, the Department of Civil and Environmental Engineering at Carnegie Mellon University has acquired a Z+F (Zoller + Frohlich) laser scanning system for use in one of the investigators' research programs.

While it is that both instruments emit laser radiation so that it is reflected back by a target of interest to an on-board receiver, there are several practical differences. The CYRAX scanner is based on time-of-flight principles while the Z+F scanner uses phase-based technology to acquire data. Since phase-based technology utilizes a continuous laser beam (whereas the time-of-flight technology uses a pulsing laser beam), the data acquisition process is much faster in the former case and thus total data acquisition times may be reduced. This aspect of performance may be important under certain conditions when fast data collection and assessment are critical. In addition, the CYRAX system employs a 1mW (green) laser while the Z+F system employs a 23mW (red) laser. These differences in laser radiation wavelength and power may be important in relation to the performance of the scanners in less than optimal scanning environments (i.e. when scanning through smoke and dust); this is currently being investigated.

These two scanning technologies are also different in terms of their ambiguity intervals, vertical and horizontal fields of view, accuracies and resolutions. These differences are important to experiment with due to the need for high-speed data collection over long ranges as well as the need for high accuracy of the data collected to enable detailed computational analysis. An evaluation of the technological feasibility and process applicability of both scanners, for the unique characteristics of the data collection and analysis issues associated with the research program, is outlined below.

With regard to validating the laser scanning technologies, three scanning sessions have taken place following the notice to proceed; two involving the Z+F system only (at the Monongahela River and Birmingham bridges) and one involving both the Z+F and CYRAX systems (at the Washington County Bridge, the chosen subject bridge structure). As indicated in the above discussion, it is confirmed that the Z+F scanning system outperforms the CYRAX system in terms of raw scanning time requirements; considering the Washington County Bridge scan, the time required by the Z+F team was four to six hours where the CYRAX team required roughly eight to twelve hours to acquire comparable point cloud data sets. This is in part due to the nature of the scanning technologies (as discussed above), but also due to the preparatory work required of the CYRAX team with regard to the on-site scanner and target layout, etc.

In furthering the progress in this research program, it is apparent that the primary time-intensive process is the analysis and registration of the acquired point cloud data sets; a process for which Geomagic v8 is currently being utilized. It is expected that a certain amount of error is present throughout the point cloud data, regardless of the scanning system utilized; however, noise-reducing algorithms coded into Geomagic serve to eliminate, or dramatically reduce unwanted noise. The preceding point is where a major difference is seen between the CYRAX and Z+F systems; a difference which ultimately results in the CYRAX system being identified as being the more desirable of the two scanners for this particular application. Justification of the foregoing follows subsequently.

First, it was found that when considering an edge-on view of a scanned surface (or a beam cross-section), a point distribution that appears Gaussian in nature is present throughout the Z-F data sets. An example of this behavior in the data set is illustrated in Figure 1 (point cloud data for a two foot length of a fascia girder from the Washington County Bridge) where a dense concentration of points occurs at the assumed surface location (i.e. mean); subsequent outliers decrease in frequency as the distance from the actual surface location increases. While this type of point distribution lends itself to the application of a best-fit plane to represent the surface, Geomagic bases these planes on three points (chosen by the user); this ultimately results in a considerable amount of work to assemble the bridge model in its entirety (this runs counter to the imperative of identifying an automatic means for model construction). Also, best-fit planes are often idealizations of curved surfaces (i.e. through the fitting of non-uniform rational B-splines, NURBs), and considering the emphasis being placed on the damaged geometry of individual components, it is not at all in the best interest of this research program to utilize this method of data registration wherein averaged geometry is employed since such an approach may have the unwanted effect of diminishing, or smoothing out, actual damage that is important to quantify within the context of any subsequent nonlinear finite element modeling.

Beyond the random variation in point ranging of bridge cross-sectional geometry that occurs in the Z+F point cloud data, this data also proves to be much less uniform than that found in the CYRAX system. This feature is made apparent in Figure 2 as the data appears to occur in waves in several locations (presumably an unwanted artifact of the scanning methodology and site conditions) while displaying obvious discontinuities in other locations. Where these discontinuities may be accounted for through multiple scans, the algorithms inherent to Geomagic do not execute properly as common surfaces and / or points are difficult to resolve; a problem that persists in much of the Z+F data acquired to date.

Following the application of relatively aggressive noise-reducing algorithms to the Z+F point cloud data sets, these localized discontinuities are often eliminated; however, global deviations within surfaces which are known to be planar in nature (concrete pier caps, etc.) are found to be on the order of one inch. Given a complete solid model with relatively frequent deviations of this nature, it is deduced that the behavior of said solid model, undergoing “virtual load testing” through the use of ADINA, would scarcely represent reality. To further complicate this issue, the raw geometrical features inherent to the damaged regions of the structure could be dramatically underestimated and / or overestimated, essentially defeating the purpose of the technique being developed.

However, while the CYRAX system nearly doubles the up-front time requirements for initial data collection at the accident site, (as compared with the Z+F system) registration of the subsequent data not only requires significantly less effort, but also results in a much more representative model. This simply appears to be the result of a lack of relative noise both at the local as well as at the global level. This result also provides a back-up with regard to the registration of multiple scan data sets since common surfaces and / or points are readily found in Geomagic; where the primary method of data set registration employs the use of predefined targets for orientation of the point cloud data sets.

Following the application of several, less aggressive noise-reducing algorithms, to the CYRAX point cloud data sets, the resultant solid model appears to be much more representative of reality; with errors in fidelity with real geometry of roughly one order of magnitude less than that found with the Z+F system. Figures 3 through 5 display CYRAX derived models employing the mentioned level of noise reduction. Two key points of interest are highlighted in these figures, however: missing data and surfaces not in the line of site of the scanner (occluded surfaces).

With regard to the missing data, two solutions have been developed to remedy this situation. The first solution is simply to perform additional scans so as to not only include data taken from underneath the superstructure, but also to include data taken from above (or at the same level) as the superstructure; in this way, so-called occluded surfaces are eliminated. The second solution is to

simply “fill in” gaps in the data using Geomagic; a relatively time intensive and inaccurate method when considering large gaps in data. While it would seem that the combination of these two solutions could lead to errors throughout the model, it must be noted that the regions of interest (i.e. the damaged regions throughout the structure) are primarily located on the fascia girders; locations which, in general, provide for full access by way of embankments, limited equipment, etc. Therefore, regions of interest have the ability to be fully scanned while those of less importance can be approximated, keeping in mind the nature of the existing structure and its as-built configuration depicted on plans.

In summary, despite the longer time required for initial acquisition of damaged bridge topologies required for the CYRAX scanner (as compared with the Z+F scanner), the quality and fidelity of the data result in significantly less labor in terms of registration and noise reduction. The quality of the scanned data is of great importance to the current research since an automation of the process is sought to reduce assessment times, ensure reproducibility in results, and ensure validity of predicted reserve capacities in the damaged bridge structures considered. In light of these points, it now appears that the CYRAX scanner is best suited to for future work in developing a successful rapid assessment technology for the Commonwealth.

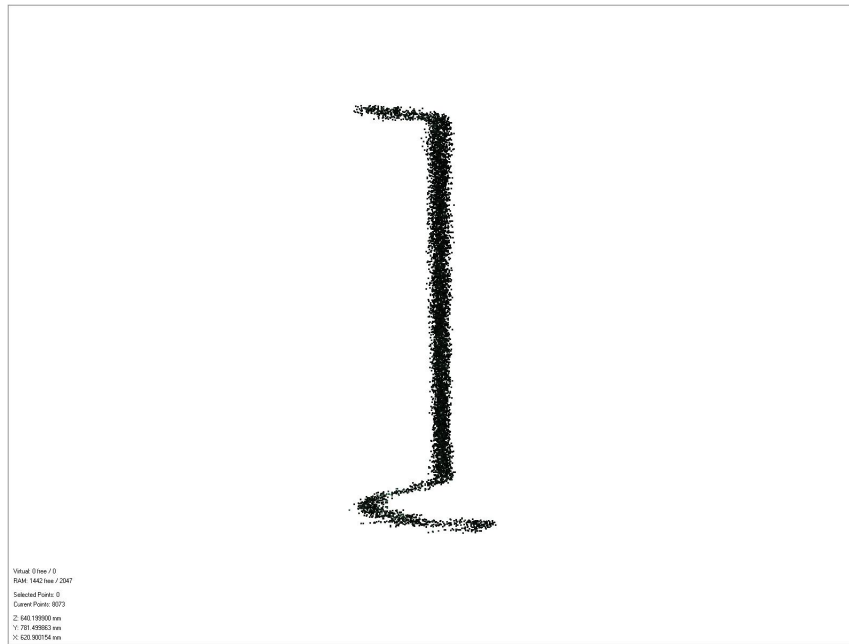


Figure 1: Edge-on view of steel I-girder point cloud data set produced with Z+F laser scanner.

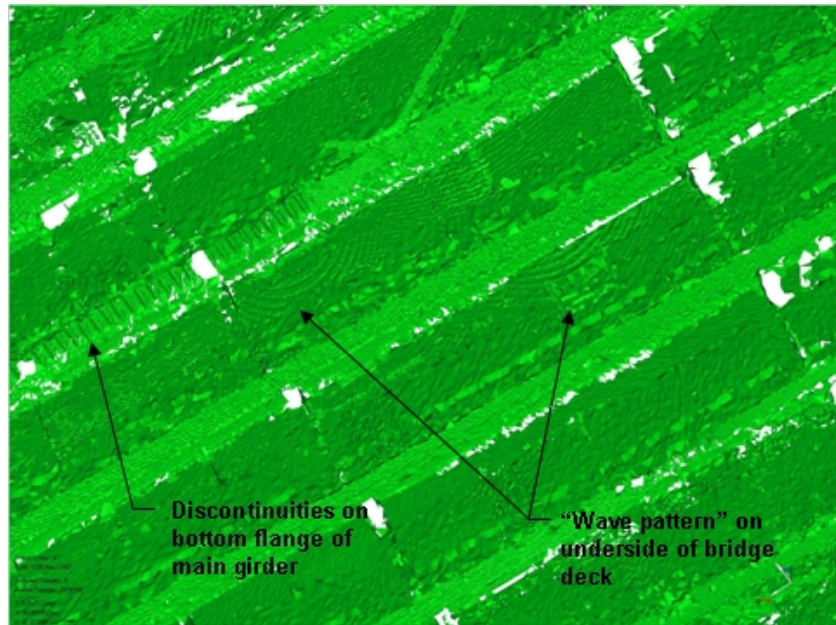


Figure 2: Discontinuities present in sample scan data from Z+F laser scanner.

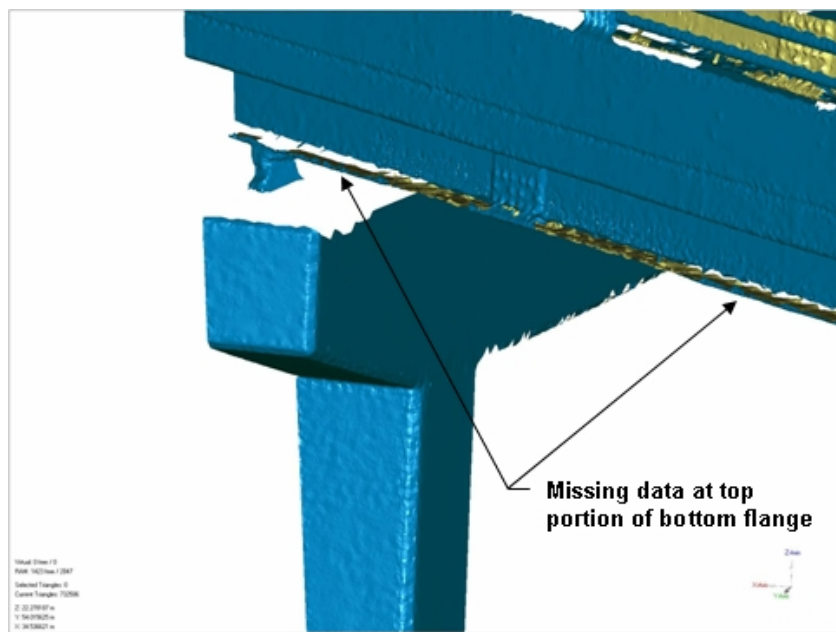


Figure 3: Tessellated surface of pier and fascia girder (with parapet wall).

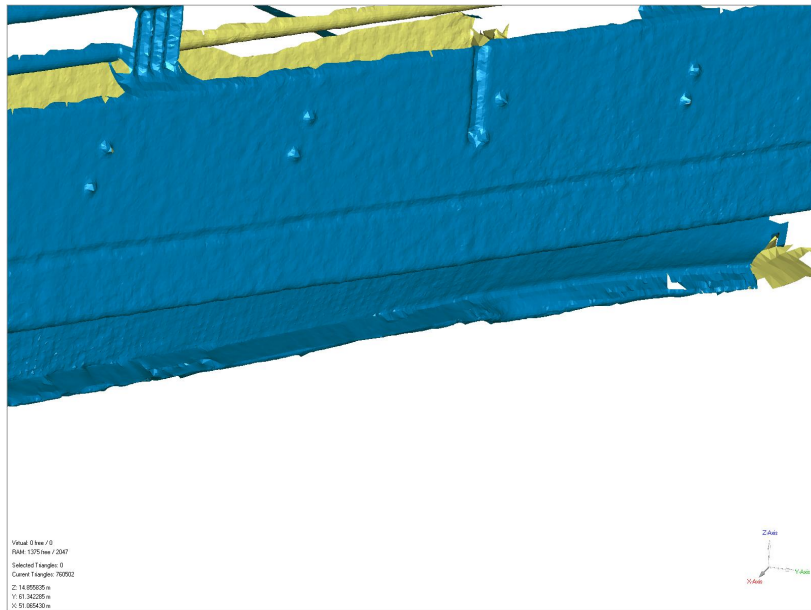


Figure 4: Close-up view of damaged region on fascia girder.

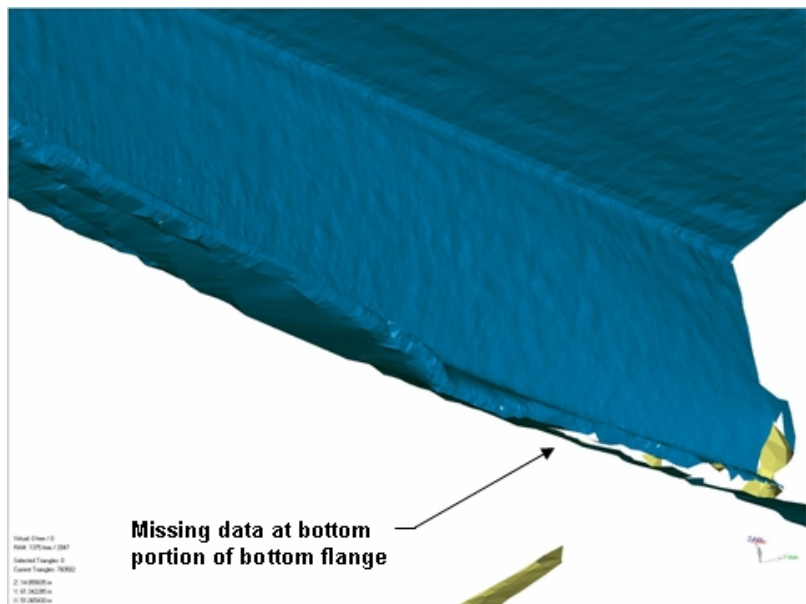


Figure 5: Underside of damaged region on fascia girder.